Shear velocity evidence of upper crustal magma storage beneath Valles Caldera

Justin Wilgus[1], Brandon Schmandt[1], Ross Maguire[1], Chengxin Jiang[2], and Julien Chaput[3]

[1]University of New Mexico
[2]Australian National University
[3]University of Texas El Paso

November 24, 2022

Abstract

Valles Caldera was formed by large rhyolitic eruptions at ˜1.6 and 1.23 Ma and it hosts post-caldera rhyolitic deposits as young as ˜70 ka, but the contemporary state of the magmatic system is unclear. Local seismicity beneath Valles Caldera is rare and shear-velocity (Vs) structure has not been previously imaged. Here, we present the first local Vs tomography beneath Valles Caldera using ambient noise Rayleigh dispersion from a ˜71 km transect of nodal seismographs with mean spacing of ˜750 m. An ˜6 km wide low-Vs anomaly (Vs<2.1 km/s) is located at ˜3-10 km depth within the 1.23 Ma caldera's ring fracture. Assuming magma in textural equilibrium, the new tomography suggests that melt fractions up to ˜17-22% may be present within the upper crustal depth range where previously erupted rhyolites were stored.

Geophysical Research Letters

Supporting Information for

Shear velocity evidence of upper crustal magma storage beneath Valles Caldera

Justin Wilgus[1](jwilgus@unm.edu), Brandon Schmandt[1], Ross Maguire[1,2], Chengxin Jiang[3], Julien Chaput[4]

1. University of New Mexico, Department of Earth & Planetary Sciences, Albuquerque, NM, USA

2. University of Illinois Urbana-Champaign, Department of Geology, Urbana, IL, USA

3. The Australian National University, Research School of Earth Sciences, Acton, ACT, Australia

4. University of Texas at El Paso, Department of Geological Sciences, El Paso, TX, USA

Contents of this file

Figures S1 to S8 Tables S1 to S3

Introduction

The supplementary information provided here includes 8 figures and 3 tables. These materials expand on processing, methodology, and results.

Figure S1. Vs search range, model parameterization, and example sensitivity kernels.

Figure S2. Number of interstation phase velocity measurements used at each period for phase velocity tomography.

Figure S3. Chi-squared ($?^2$) misfit maps.

Figure S4. Uncertainty test cases and their BMMC inversion results.

Figure S5. Phase velocity resolution test at 4 s with strongly reduced velocities within the ring fracture of the caldera.

Figure S6. Phase velocity resolution test at 4 s period with alternating positive and negative velocity anomalies surrounded by neutral velocities.

Figure S7. Phase velocity predictions and Vs profiles of the 2,000 best BMMC models for three points across the transect.

Figure S8. Vs as a function of melt fraction over aspect ratios indicative of textural equilibrium, 0.1 to 0.15.

Table S1. List of stations that tipped at some point during deployment.

Table S2. Prior velocity range for each b-spline parameter in BMMC inversion.

Table S3. Weight percent bulk major oxide compositions from Banco Bonito rhyolite flow.

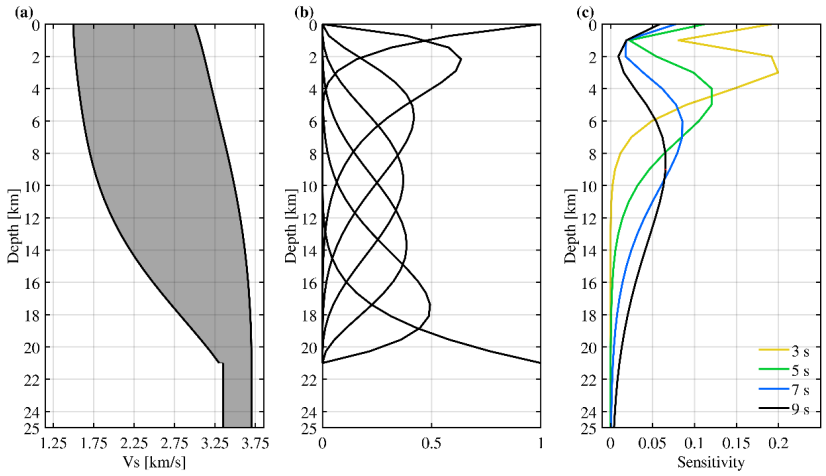

Figure S1. Figure S1. Vs search range, model parameterization, and example sensitivity kernels. a) A uniform prior Vs distribution was used within search range indicated by gray shading. b) The shape of the 7 b-spline functions used to parameterize the middle to upper crust is shown with solid black lines. The plots in a and b use a depth to half-space of 21 km. That depth was allowed to vary from 20-23 km in the inversion. C) Phase velocity sensitivity to Vs structure at periods of 3, 5, 7, and 9s calculated from the mean Vs profile (Figure 3) using SensKernel-1.0 (Levshin et al., 1989). Note that the BMMC inversion does not use these kernels; it accounts for nonlinearity by repeated forward modeling. The example kernels are shown here to help illustrate the typical sensi tivity of the phase velocity measurements.

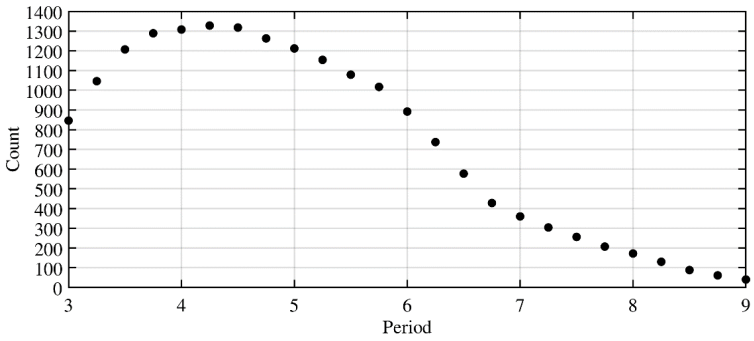

Figure S2. Number of interstation phase velocity measurements used at each period for phase velocity tomography along the transect.

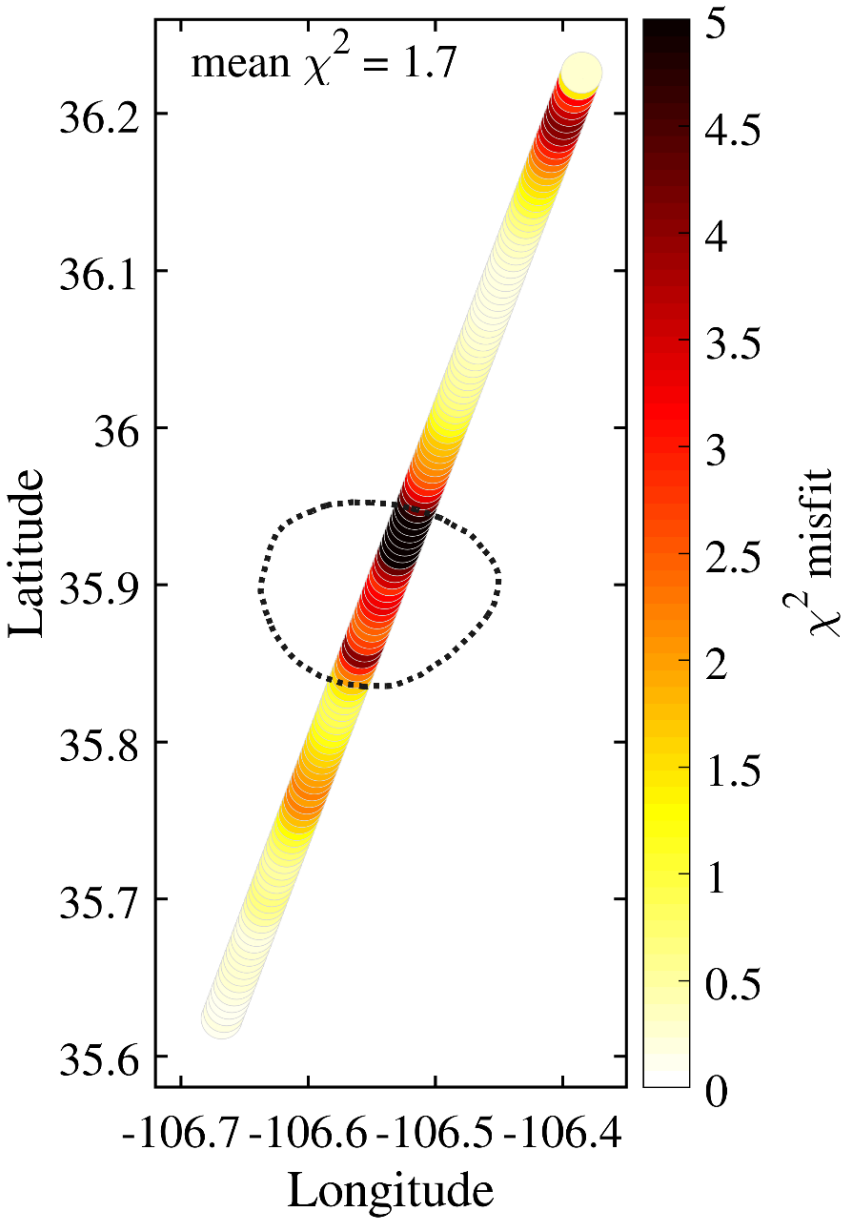

Figure S3. Map of average X2 misfits from the posterior distribution at each Vs inversion location. The mean misfit of all locations, 1.7, is given in the plot.

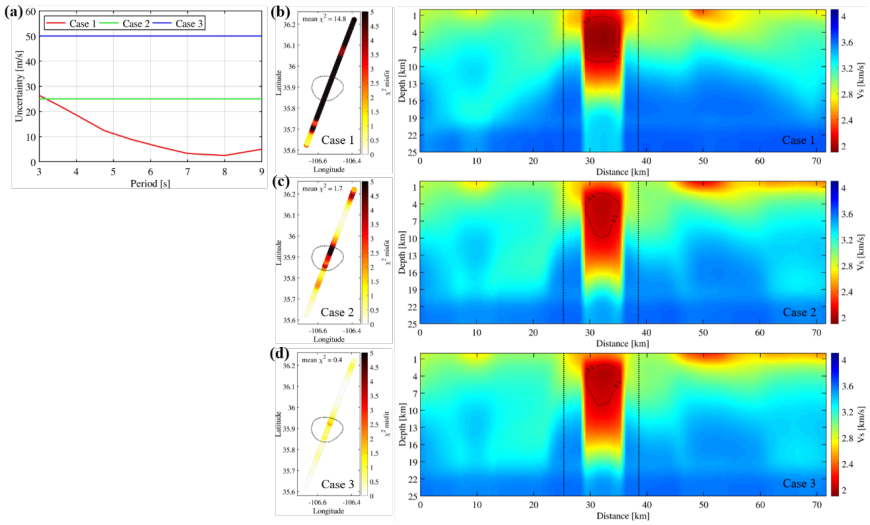

Figure S4. Uncertainty test cases and their BMMC inversion results. a) Uncertainties for each of the three cases. Case 1 uses uncertainties from bootstrap resampling of the phase velocity results and repeated inversions with the bootstrap samples. Case 2 uses a fixed 25 m/s uncertainty at all periods, which is the case presented in the main text. Case 3 uses a fixed 50 m/s uncertainty range. b) Misfit map and Vs cross section for case 1. c) same as b but for case 2. b) same as c but for case 3. Dotted lines in misfit maps and Vs cross section show the 1.23 Ma caldera's ring fracture.

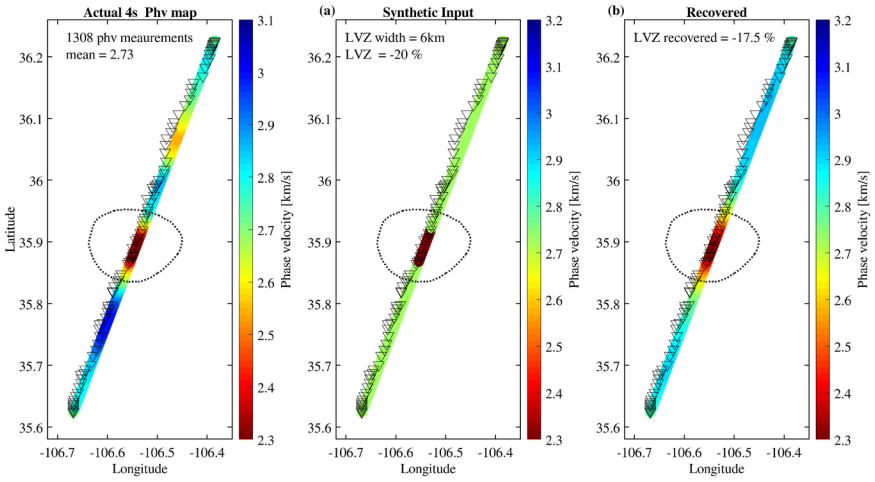

Figure S5. Phase velocity resolution test with strongly reduced velocities within the ring fracture of the caldera. a) The input structure includes a 6-km wide low-velocity anomaly with 4-s Rayleigh wave phase velocity reduced by 20%. For reference, the observationally estimated phase velocity anomaly at 4 s period is ˜15% so this test is using a more severe anomaly. b) The recovered phase velocities from the inversion of synthetic data show that a peak velocity reduction of –17.5% is recovered. Thus, ˜85% of the magnitude of the input anomaly was recovered

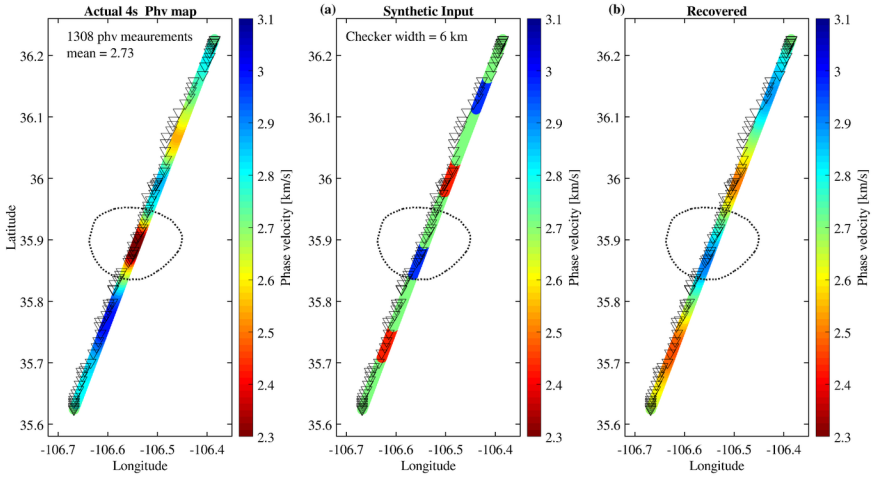

Figure S6. Figure S6. Phase velocity resolution test at 4 s period with alternating positive and negative velocity anomalies surrounded by neutral velocities. a) The input structure contains 10% velocity anomalies that are 6-km wide and separated by equal-widths of neutral velocities. b) All four input anomalies are recovered with slightly reduced magnitudes, but the anomalies within the interior of the transect are better resolved than those closer to the edges.

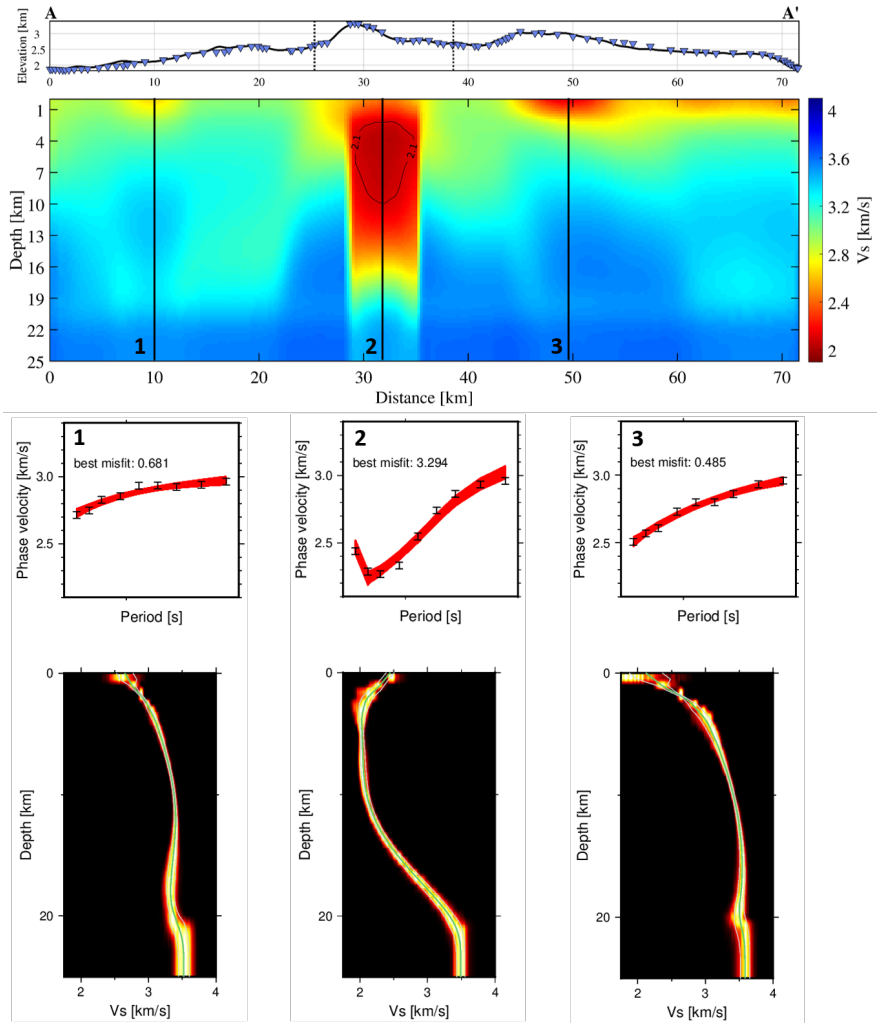

Figure S7. Phase velocity predictions and Vs profiles of the 2,000 best BMMC models for three points across the transect.

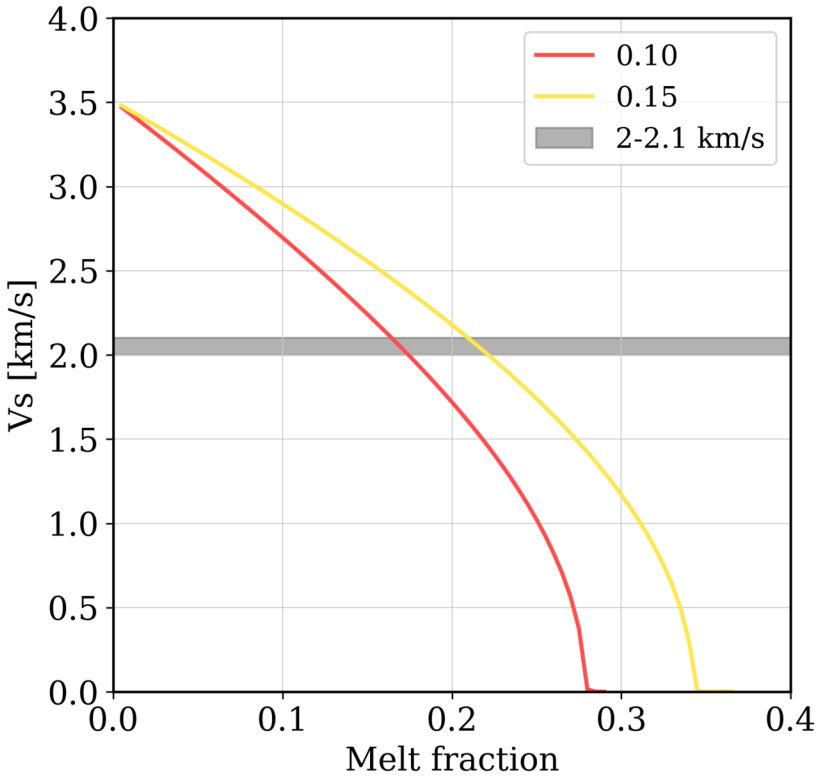

Figure S8. Vs as a function of melt fraction over aspect ratios indicative of textural equilibrium, 0.1 to 0.15. Solid phase Vs values were determined using the ˜70 ka Banco Bonito rhyolite composition at 170 MPa (˜5 km depth), and 700 C°. A density of 2.2 kg/m3 and bulk modulus of 9 GPa were assumed for the melt phase.

Station name	Latitude	Longitude	Approximate day of tip
28	35.89744	-106.5471	Before 10-10-2019
33	35.93139	-106.5132	Before 10-10-2019
37*	35.97542	-106.5064	10-30-2019
1011	35.86139	-106.563	Before 10-10-2019
1015	35.87358	-106.5505	Before 10-10-2019
1017*	35.88239	-106.548	10-20-2019
1019	35.92355	-106.5313	Before 10-10-2019
1020	35.93081	-106.5302	Before 10-10-2019
1024*	35.96445	-106.5131	10-20-2019
1027	35.99831	-106.4988	10-10-2019

Table S1. List of stations that tipped at some point during deployment. Stations with asterisk recorded >10 days of data that were used for ambient noise cross correlations. The other tipped stations were not included in our analysis.

Spline #	Lower bound	Upper bound
1	1.50	3.00
2	1.50	3.10
3	1.60	3.25
4	1.70	3.55
5	1.95	3.65
6	2.90	3.70
7	3.30	3.70

Table S2. Prior velocity range for each b-spline parameter in BMMC inversion.

Oxide	Weight%
SiO2	74.2
AI2O3	13.24
Fe2O3	1.82
MgO	0.67
CaO	1.49
Na2O	3.85
K2O	4.36

Table S3. Weight percent bulk major oxide compositions from Banco Bonito, the youngest rhyolite flow at Valles caldera (Fig. 1; Spell and Kyle, 1989).

Hosted file

`essoar.10512567.1.docx` available at https://authorea.com/users/549881/articles/603773-shear-velocity-evidence-of-upper-crustal-magma-storage-beneath-valles-caldera

Shear velocity evidence of upper crustal magma storage beneath Valles Caldera

Justin Wilgus[1] (jwilgus@unm.edu), Brandon Schmandt[1], Ross Maguire[1,2], Chengxin Jiang[3], Julien Chaput[4]

1. University of New Mexico, Department of Earth & Planetary Sciences, Albuquerque, NM, USA

2. University of Illinois Urbana-Champaign, Department of Geology, Urbana, IL, USA

3. The Australian National University, Research School of Earth Sciences, Acton, ACT, Australia

4. University of Texas at El Paso, Department of Geological Sciences, El Paso, TX, USA

Key points

- The Valles Caldera magmatic system was imaged with ambient noise Rayleigh tomography using a dense temporary seismic transect.
- A low-Vs anomaly, Vs<2.1 km/s is imaged within the caldera's ring fracture at ~3-10 km depth.
- The upper crustal magma reservoir beneath Valles caldera may contain up to ~17-22% rhyolitic melt.

Abstract

Valles Caldera was formed by large rhyolitic eruptions at ~1.6 and 1.23 Ma and it hosts post-caldera rhyolitic deposits as young as ~70 ka, but the contemporary state of the magmatic system is unclear. Local seismicity beneath Valles Caldera is rare and shear-velocity (Vs) structure has not been previously imaged. Here, we present the first local Vs tomography beneath Valles Caldera using ambient noise Rayleigh dispersion from a ~71 km transect of nodal seismographs with mean spacing of ~750 m. An ~6 km wide low-Vs anomaly (Vs<2.1 km/s) is located at ~3-10 km depth within the 1.23 Ma caldera's ring fracture. Assuming magma in textural equilibrium, the new tomography suggests that melt fractions up to ~17-22% may be present within the upper crustal depth range where previously erupted rhyolites were stored.

Plain Language summary

Silica-rich magma stored in the shallow crust of the Earth can fuel eruptions that pose significant hazards to society. Valles Caldera was created by a large explosive eruption of silica-rich magma 1.23 million years ago. Numerous smaller volcanic eruptions occurred following the large eruption event (as young as 70 thousand years ago) and the shallow subsurface at Valles remains hot indicating potential for modern magmatic storage at depth. Seismic shear waves are sensitive to the presence of magma and other variations in crustal structure. However,

no local shear wave imaging has been conducted at Valles Caldera. Using new seismic data from densely spaced instruments and a technique known as ambient noise tomography, we produced the first shear velocity image beneath Valles Caldera. A region of significant low shear velocity is present in the upper crust beneath the caldera which we attribute to the presence of silica-rich magma. These new results on shallow magma storage can contribute to assessing volcanic hazards more accurately near Valles Caldera.

1. Introduction

Understanding the current state and evolution of caldera-forming magmatic systems is an important challenge because these systems exhibit diverse life-cycles with a wide variety of hazardous eruptive scenarios (Cashman and Giordano, 2014; Wilson et al., 2021). Valles Caldera was formed by two rhyolitic eruptions that each deposited >300 km^3 dense rock equivalent (DRE) at ~1.6 and ~1.23 Ma, respectively (Goff et al., 2014; Cook et al., 2016; Wu et al., 2021; Nasholds and Zimmerer, 2022). It is often considered the type example of a resurgent caldera with a central dome, Redondo Peak, that was uplifted within ~54 kyr of the last caldera-forming eruption and peripheral post-caldera rhyolite flows following the contour of its ring fracture (Figure 1; Smith and Bailey, 1968; Philips et al., 2007; Kennedy et al., 2012). The clarity of its geological record of caldera-forming processes contrasts with the uncertain contemporary state of the underlying magmatic system.

Post-caldera volcanism primarily occurred between ~1.23 - 0.5 Ma and the subsequent quiescence was interrupted by eruption of the ~74 ka El Cajete pyroclastic deposits and ~68 ka Banco Bonito rhyolite flow near the southwestern moat of the caldera (Philips et al., 2007; Zimmerer et al., 2016). Petrologic evidence suggests that the Banco Bonito lavas were generated by renewed intrusion of more mafic melt (Wolff and Gardner, 1995). The potential occurrence of more recent magma recharge is unresolved. A lack of contemporary seismicity beneath Valles Caldera may indicate a stable cooling reservoir or primarily ductile deformation due to high crustal temperatures (Sanford et al., 1979; House and Roberts, 2020; Nakai et al., 2017). Boreholes drilled for geothermal exploration and basic science document high geothermal gradients of up to ~350-450 °C/km just west of the caldera's center (Figure 1; Morgan et al., 1996). Most boreholes within the caldera encountered high-temperature alteration but a dearth of magmatic fluids suggesting a shrinking hydrothermal system (Nielson and Hulen, 1984; Goff and Gardner, 1994). Broader analysis of shallow hydrothermal fluids within and surrounding Valles Caldera indicates ongoing transport of mantle-derived helium consistent with input of mafic melts at depth (Goff and Janik, 2002; Blomgren et al., 2019).

Seismic imaging provides insight into the contemporary abundance of magma in the upper crust beneath Valles Caldera. Early P-wave studies indicated low P-velocity (Vp) and elevated attenuation beneath the caldera (Ankeny et al., 1986; Roberts et al., 1991, 1995). Teleseismic P-wave data from the 1993-1994 Jemez Tomography Experiment (JTEX) enhanced resolution within the caldera and

revealed a low-Vp anomaly between ~5-20 km depth in the shape of a vertically elongated ellipsoid with a Vp reduction of -23% (Steck et al., 1998). Following JTEX, there was a long hiatus in data collection for local imaging. Denser arrays and application of newer seismic methods such as ambient noise surface wave tomography could add valuable S-velocity (Vs) constraints with complementary sensitivity to melt, improved depth-resolution, and better facilitate comparison of Valles Caldera to other systems that may be in a similar life-cycle stage (e.g., Schmandt et al., 2019).

Here, we present the first local Vs tomography beneath Valles Caldera by applying ambient noise Rayleigh wave tomography to data from a new dense seismic transect (Figure 1). Short-period Rayleigh wave dispersion constrains absolute Vs in the middle to upper crust and the mean seismograph spacing of ~0.75 km provides the ability to recover local variations in structure along the ~71-km transect. The new Vs tomography results are used to estimate the potential depth interval and concentration of magma beneath Valles Caldera.

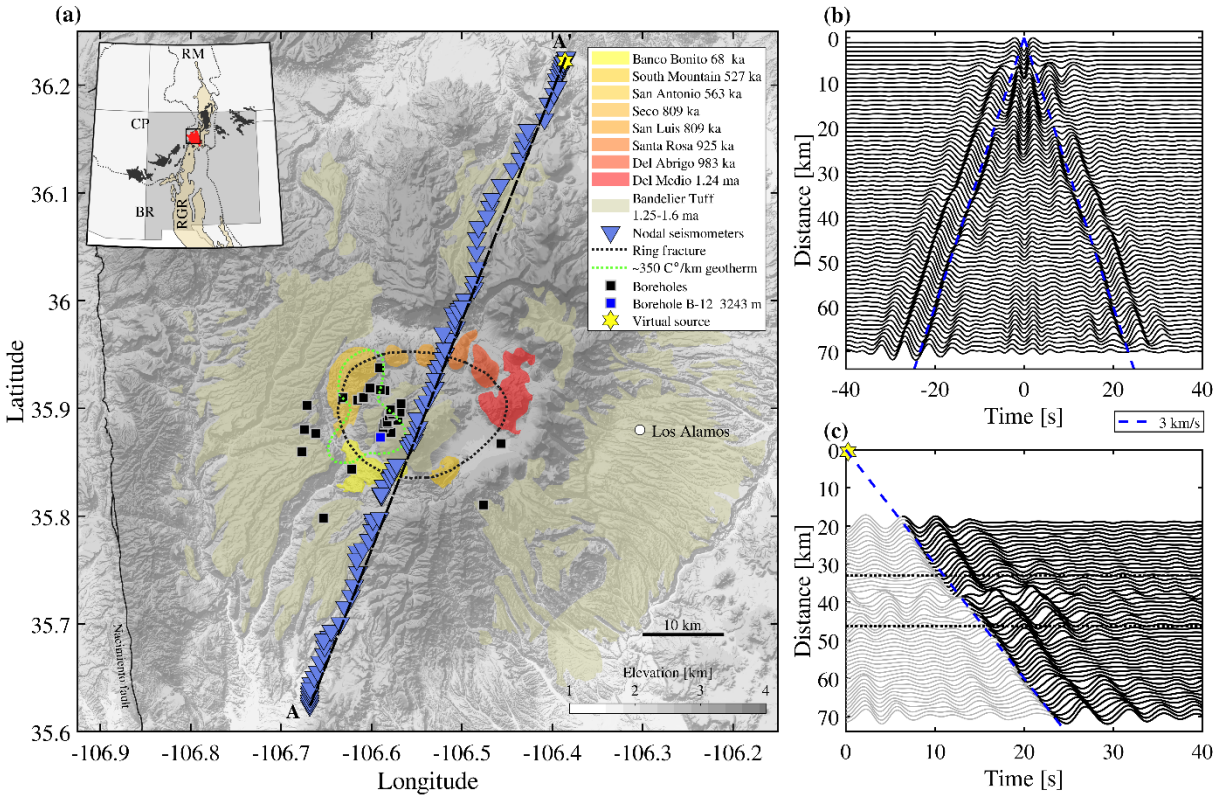

Figure 1. Study area map and example data. a) A topographic map centered on Valles caldera is shown with semi-transparent fill indicating major rhyolitic outflows colored by time of eruption. Blue triangles are nodal seismographs. A black dotted line shows the surficial trace of the ring fracture from the 1.23 Ma

eruption. The green dotted line encloses the area with 350° C/km geothermal gradient (Morgan et al., 1996) and squares are borehole locations. Borehole B-12 is the deepest at ~3.2 km. A yellow hexagram shows the virtual source used in panel c. Line, A-A', delineates the tomographic cross section. The left inset shows regional physiographic provinces: Colorado Plateau (CP), Basin and Range (BR), Rocky Mountains (RM), and Rio Grande Rift (RGR). Semi-transparent tan fill shows the RGR. Solid black fill shows Cenozoic volcanic fields of the Jemez lineament. Solid red fill shows the Jemez volcanic field which includes Valles Caldera and the black square outlines the extent of the main figure. b) Noise cross correlations are shown filtered from 3-9 s and stacked at a distance interval of 1 km. c) A virtual source gather is shown using a northern station and 3-5 s bandpass filter. Black dotted lines denote the 1.23 Ma caldera's ring fracture.

2 Data and Methods

2.1 Data

Continuous seismic data was recorded with 97 three-component Magseis-Fairfield nodal seismometers. The stations were deployed along a ~71 km NNE striking linear transect across Valles Caldera (Figure 1) with a spacing of ~750 m and operated between September 29, 2019, and November 9, 2019. The nodal seismographs were coupled to the ground with stakes but not buried to minimize environmental impact. Ten seismographs tipped during deployment, presumably due to wildlife interactions based on frequent observations of elk and cattle. Three of the tipped stations had >10 days of data that were recovered by identifying the day that inter-station noise correlations abruptly changed. Tipped nodes are noted in the Supporting Information (Table S1).

2.2 Ambient noise correlations

Ambient noise cross-correlation functions were calculated from ambient seismic noise following Bensen et al., (2007). The data were down-sampled to 10 Hz, bandpass filtered from 0.02 - 2 Hz and whitened before cross-correlation. Correlations were computed for 4-hour half-overlapping time windows throughout the continuous data (e.g., Seats et al., 2012) and then all correlations for each station pair were linearly stacked. We focus on the vertical-vertical (ZZ) component cross-correlations which show clear fundamental mode Rayleigh waves on the positive and negative lag portions of the symmetric cross correlations (Figure 1b).

2.3 Phase velocity dispersion

Phase velocity dispersion curves were calculated using the automated frequency-time analysis (FTAN) method (Levshin et al., 1972; Bensen et al., 2007). We focus on 3-9 s periods that are sensitive to the upper and middle crust (Figure S1 in Supporting Information). Below 3 s period clear fundamental mode Rayleigh waves were not observed. Beyond 9 s period the ~71-km long transect provides few measurements with inter-station spacing greater than our minimum of 1.5

wavelengths. To boost the signal-to-noise ratio as well as to reduce the potential effects of inhomogeneous noise source distribution, we averaged the positive and negative portions of the cross-correlation functions. We retained measurements with phase velocities between 1 and 4.6 km/s, SNR > 5, and wavelengths > 1.5, resulting in 2,749 total dispersion curves available for phase velocity tomography.

2.4 Phase velocity tomography

A damped least-squares method was used to invert inter-station phase velocity dispersion measurement for phase velocity along the transect for periods between 3-9 s (e.g., Wilgus et al., 2020). At 4 s period there are ~1,300 inter-station phase velocity measurements used for tomography. This number decreases with increasing period as the 1.5 wavelength requirement becomes a larger fraction of array length (Figure S2 in Supporting Information). The inversion was conducted with straight rays on a 0.5 km grid along linear transect A-A' shown in Figure 1. To reduce the influence of potential outliers among the dispersion measurements, a two-stage inversion approach was used in which measurements with travel time residuals beyond two standard deviations after the first inversion were removed and then the inversion was repeated (e.g., Wang et al., 2017).

2.5 Shear velocity inversion and modelling

Phase velocity dispersion curves from 3-9 s period were extracted for 144 locations along the transect to invert for Vs as a function of depth. We closely followed the workflow of Wilgus et al., (2020) using a Bayesian Markov chain Monte Carlo (BMMC) approach to obtain an ensemble of Vs models capable of fitting the dispersion measurements (Shen et al., 2013). The subsurface Vs structure is represented by a total of 9 parameters, consisting of 7 b-splines for Vs in the middle to upper crust, a depth transition to an underlying half-space at 20-23 km, and Vs in the half-space. To accommodate potentially strong heterogeneity in the upper crust and diminishing resolution with depth, the prior distribution is wider in the upper crust and narrows with depth (Figure S1 and Table S2 in Supporting Information). Phase velocity sensitivity kernels show that 90% of the sensitivity for the longest period Rayleigh wave, 9 s, is located above 21 km depth. Consequently, the parameterization transitions from 7 b-splines to a half-space within a depth range of 20-23 km (Figure S1 in Supporting Information). The BMMC inversion explores the model space, iteratively predicting dispersion (p_i), and evaluating the fit to the observed dispersion (d_i) with a reduced Chi-squared misfit equation $\chi^2 = n^{-1} \sum_{i=1}^{n} \ _i^{-2} \left(d_{\mathrm{i}} - p_i\right)^2$, where is uncertainty and n is the number of discrete periods. A total of 2 million iterations were used at each point along the transect. The best 2,000 models at each location are used as the posterior distribution and the mean of the ensemble is used for constructing the final Vs profile. All forward calculations of phase velocity were conducted with software from Computer Programs in Seismology (Herrmann, 2013) using empirical crustal rock scaling relationships between Vs, Vp, and density (Brocher, 2005).

Multiple estimates of phase velocity uncertainty were tested in the Vs inversions. We chose to use a fixed value of 25 m/s, which results in a mean Chi-squared misfit of 1.7 (Figure S3 in Supporting Information). An alternate approach using bootstrap resampling and repeated phase velocity tomography (e.g., Jiang et al., 2018) resulted in smaller uncertainties and a greater mean Chi-squared misfit of 14.8. Results based on different uncertainty choices show that the geometry of major features of the model is stable but small variations in the amplitude of velocity anomalies are present (Figure S4 in Supporting Information). For instance, using the smaller uncertainties from the bootstrap approach results in a slightly lower minimum Vs of ~1.95 km/s rather than ~2.0 km/s.

2.6 Teleseismic P-wave relative delay times

The dense spacing of the nodal seismograph array provides an opportunity to observe teleseismic P-wave residual times as a simple metric of consistency with prior P-wave studies and consistency between any major Vp and Vs anomalies. However, the brief deployment did not provide many high-quality events. One of the clearest teleseismic P-waves observed when most nodes were operating is shown in Figure 2. The event occurred in Japan and the P-wave approaches Valles Caldera from the northwest. The seismograms were bandpass filtered from 0.25-0.75 Hz and aligned based on travel time predictions for the AK135 velocity model (Kennett et al., 1995). Seismograms with signal to noise amplitude ratios < 3 were removed. Relative alignment of the seismograms with multi-channel cross correlation was used to identify Vp anomalies sampled by steeply incident P-waves (VanDecar and Crosson, 1990). Since there is ~1.8 km topographic relief along the transect, we applied elevation corrections assuming an upper crustal Vp of 5.5 km/s based on estimates from controlled source and earthquake travel time tomography (Ankeny et al., 1986).

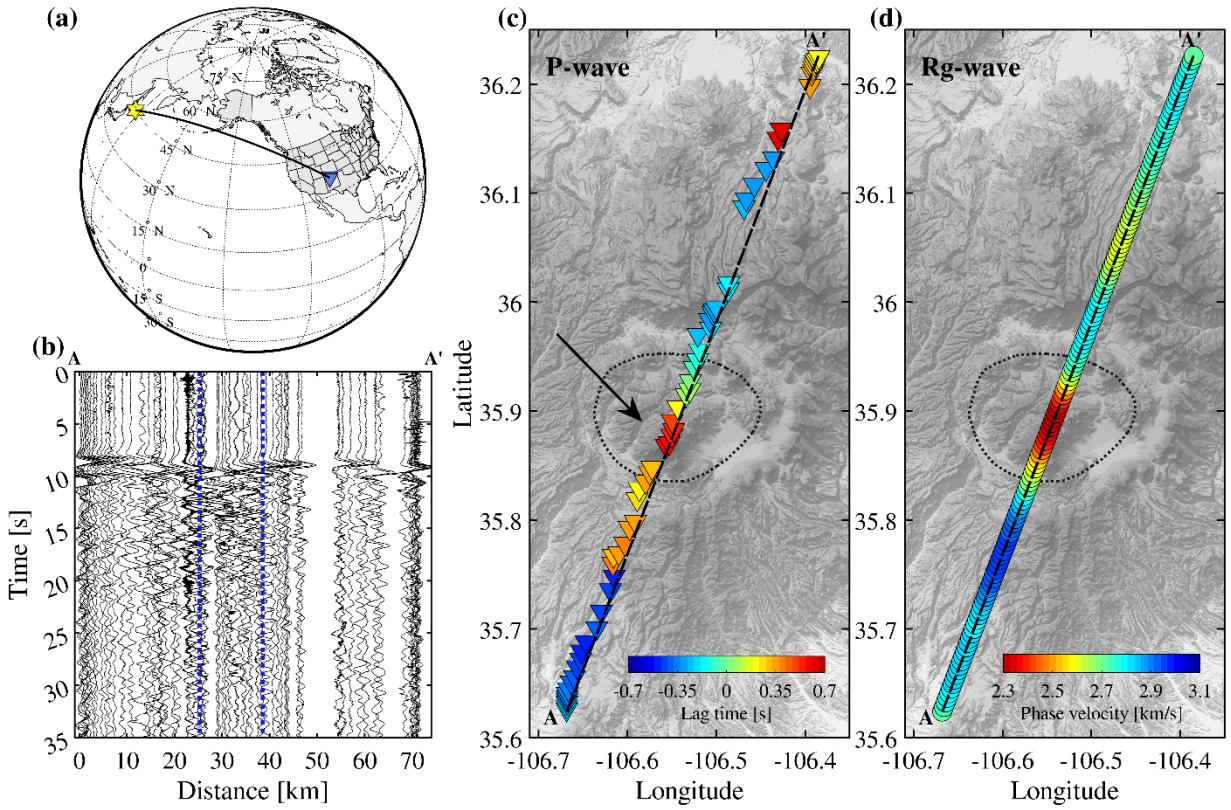

Figu

2. Comparison of teleseismic P-wave lag times and 3-5 s Rayleigh wave phase velocities. a) The map shows the M5.7 earthquake location (yellow hexagram) and the Valles transect (blue triangle). b) Waveforms are shown across the Valles transect (A-A') filtered from 0.25-0.75 Hz. Blue dotted lines denote the 1.23 Ma ring fracture. c) P-wave lag times corrected for topography. A black arrow corresponds to the incoming azimuth of the P-wave. Missing nodes were either not recording during the event or had signal-to-noise ratio < 3. d) Period averaged (3-5 s) phase velocity is plotted along A-A'.

3 Results

3.1 Phase velocity pseudo cross-section

The depth of peak sensitivity for Rayleigh wave phase velocity increases with period such that plotting the phase velocities beneath each point along the transect provides a pseudo cross-section perspective on local crustal structure (Figure 3b). The most prominent feature of the pseudo cross-section is a low-velocity anomaly for periods between ~3-5 s beneath the Redondo Peak resurgent dome, with the lowest velocity found for ~4 s period (Figure 2d and 3c). Beneath the central caldera across a width of ~6-8 km within ring fracture, 3-5 s phase velocities are ~12-15% lower than the array mean, ~2.3-2.4 km/s (Figure 2d and 3c). The

magnitude of the low-velocity anomaly makes it visible in virtual source gathers of noise correlations as a deflection in the Rayleigh wave arrival as it crosses the central caldera within the ring fracture (Figure 1c). Phase velocity tomography resolution tests demonstrate that a prominent low-velocity anomaly within the caldera's ring fracture is resolvable with the available data coverage, but the magnitude of the velocity anomaly would be slightly underestimated (Figure S5 and S6 in Supporting Information). A test with an input anomaly of –20% in phase velocity across a 6 km width resulted in a recovered minimum velocity of –17.5% (Figure S5 in Supporting Information). Other phase velocity features include low velocities (~2.5 km/s) at 3-4 s period on the northern flank of the caldera (~45-55 km transect distance) and high velocities (~3.1 km/s) at 3-4.5s on the southern flank of the caldera (~15-23 km transect distance; Figure 3b).

3.2 Shear velocity cross-section

Inversion for Vs provides constraints on absolute Vs as a function of depth. Extremely low Vs (< 2.1 km/s) is found from ~3-10 km depth across a width of ~6 km within the 1.23 Ma caldera's ring fracture (Figure 3b). The low-velocity anomaly within the Vs<2.1 km/s contour corresponds to an ~32% Vs reduction compared to the mean across the array. The anomaly's location under the Redondo Peak resurgent dome is slightly offset from the area of highest geothermal gradients, however most boreholes were drilled on the west side of Redondo Peak, whereas the nodal array crossed closer to the center of the dome (Figure 1). The highest X^2 misfit values (>4) are situated on either side of the low-Vs anomaly (Figure S3 in Supporting Information), suggesting that phase velocities near the edges of the anomaly are difficult to fit with locally 1D velocity structure. Aside from the low-velocity anomaly beneath Redondo Peak, there is a low-velocity anomaly with Vs of ~2.2-2.5 km/s on the northern flank of the caldera (transect distance of ~45-55 km), but unlike the central caldera anomaly its depth extent is restricted to the uppermost ~2 km (Figure 3c, Figure S7 in Supporting Information).

3.3 Teleseismic P-wave lag times

P-wave travel time lags of up to +/- 0.65 s were measured for a clearly recorded teleseismic earthquake (Figure 2c). A deflection in the P-wave arrival can be seen in the waveforms recorded within the caldera's ring fracture (Figure 2b). Delayed arrivals, indicative of low Vp at depth, are located on the Redondo peak resurgent dome within the Valles caldera ring fracture (Figure 2b). The location of the most delayed arrivals is consistent with previous P-wave studies that used seismographs with greater inter-station spacing but distributed over the area of the caldera rather than in one transect (Steck et al., 1998; Roberts, Aki, & Fehler, 1991). The along-transect distance of the most delayed arrivals, ~0.5-0.65 s, coincides with the area of highest geothermal gradients (Morgan et al., 1996). More moderate lag times of ~0.3 s extend south from Redondo Peak to ~10 km beyond the southern edge of the caldera (Figure 2c). The broad width of the ~0.3 s delays is consistent with a deeper origin located west of the nodal transect based on the ~315° back-azimuth of this event (Figure 2c).

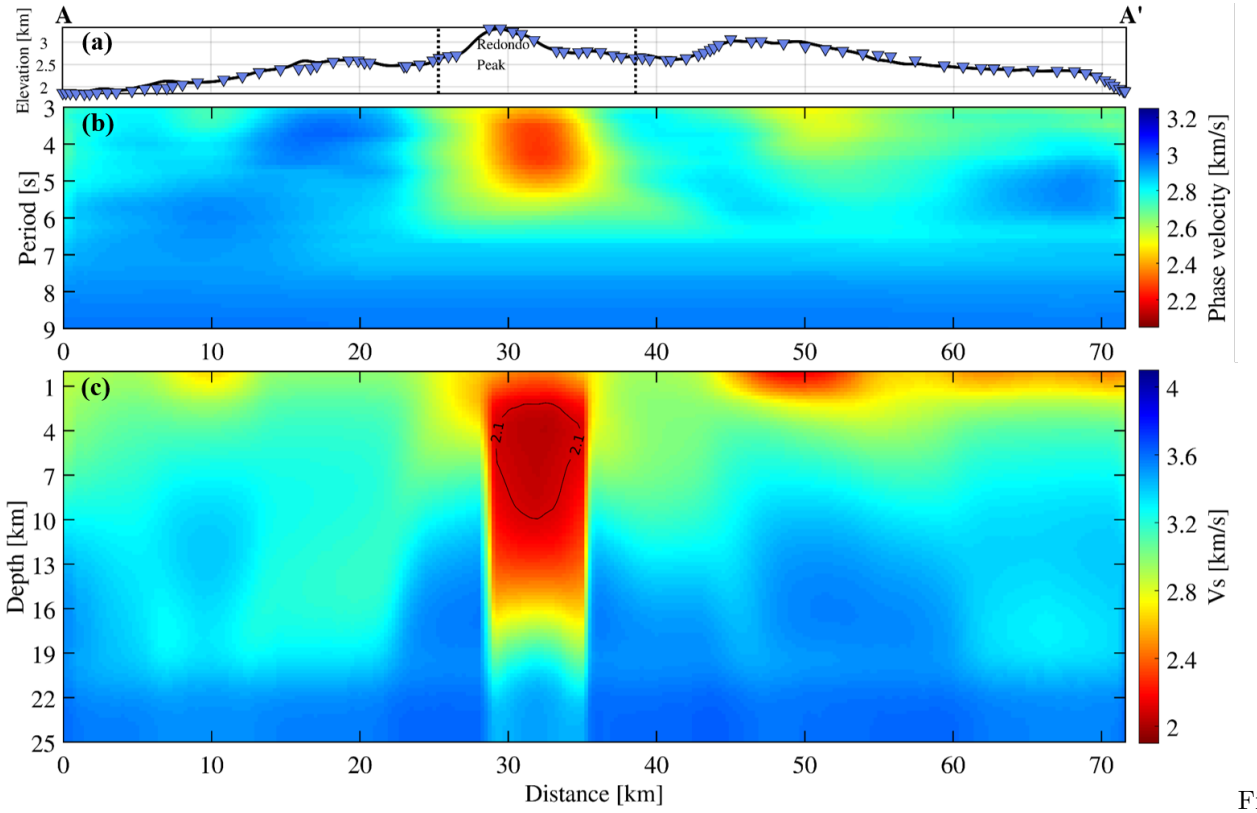

Fig

3. Tomographic cross-sectional (A-A') images of Valles Caldera. a) Smoothed topography along A-A' with 3x vertical exaggeration. Redondo Peak (labeled) is the highest elevation point of the resurgent dome. Blue triangles are seismograph locations and dotted lines show locations of the 1.23 Ma ring fracture associated with eruption of the upper Bandelier tuff (Tshirege member). b) Phase velocity as a function of period (3-9 s) is shown along the transect. c) Shear velocity is shown as a function of distance along the transect and depth beneath the surface with no vertical exaggeration.

4 Discussion

The new Rayleigh wave tomography advances insights into local Vs structure within and surrounding Valles Caldera. The primary result is strongly reduced Vs beneath the resurgent dome, Redondo Peak. A secondary low-Vs anomaly, ~2.2-2.5 km/s, located in the uppermost 2 km on the northern flank of the caldera is more likely related to the history of volcanic deposition in the area (Figure 3b). Beginning in the mid-Miocene there was intermediate-to-mafic volcanic activity on the north side of the caldera and the resulting extrusive rock deposits may cause lower Vs in the uppermost crust that contrasts with the southern flank of the caldera (Goff et al., 2011). The central caldera low-Vs anomaly and its potential implications for the contemporary state of the

magmatic system are the focus for the remainder of the discussion.

Within the caldera the lowest Vs volume is concentrated between ~3-10 km depth over a width of ~6 km within the 1.23 Ma ring fracture, where Vs is ~2.0-2.1 km/s (Figure 3b). The relative Vs anomaly within that volume is -32%. Prior teleseismic P-wave tomography estimated a relative velocity anomaly of –23% within a more vertically-elongated ellipsoidal anomaly (Steck et al., 1998). Reflectors previously identified by P-wave coda migration at ~4 km and ~9-14 km below the surface may represent the vertical boundaries of the magma reservoir, but the upper reflector may alternatively be related to the contact between tuff deposits and the underlying basement rock (Aprea et al., 2002). The availability of absolute Vs in the upper to middle crust from this study provides valuable new constraints for estimating the origin of the low-velocity anomaly. Given the Vs anomaly's location under the resurgent dome and that its minimum velocities are located between ~3-10 km depth, it cannot be explained by unconsolidated caldera fill. The depth range of the anomaly overlaps petrologically estimated storage depths of erupted rhyolites, ~2.5-9 km (Wilcock et al., 2013; Boro et al., 2020; Spell and Kyle, 1989). So, we proceed to interpret silicate partial melt and magmatic volatiles as probable contributors to the low-velocity anomaly.

We first consider a base scenario in which melt fraction is estimated assuming a composition like that of the ~70 ka Banco Bonito rhyolite flow (Table S3 in Supporting Information) and that partial melt in the subsurface today is in textural equilibrium. Then we proceed to discuss uncertainties that could lead to over- or under-estimation of the melt fraction. To predict Vs as a function of the melt fraction, we used the theoretical model of Berryman (1980) for an elastic medium with ellipsoidal fluid inclusions (e.g., Paulatto et al., 2019). Elastic properties of the solid were calculated with Perplex assuming bulk composition of the Banco Bonito rhyolite, pressure of 170 MPa (~5 km depth), and a temperature of 700 °C (Connolly, 2009). The velocity reduction due to partial melt depends on the assumed aspect ratio of intergranular melt pockets and aspect ratios of ~0.1-0.15 are expected for textural equilibrium (Takei, 2002). In this scenario, Vs of 2-2.1 km/s would correspond to melt fractions of 17-22% (Figure S8 in Supporting information). We consider textural equilibrium a reasonable assumption because the system has not erupted since ~70 ka and it hosts little seismicity, so any deformation and magmatic recharge are expected to be slowly evolving processes.

Uncertainties in seismic imaging and the multi-phase structure of the magma reservoir could bias the estimated melt fractions. This study benefits from a dense local array, but simplifying assumptions include a 2D phase velocity inversion and straight ray paths. Resolution tests using these assumptions indicate that ~85% of the input velocity anomaly amplitude could be recovered for a low-velocity anomaly like that imaged beneath Redondo (Figure S5 and S6 in Supporting Information). A surface wave tomography resolution study using 3D synthetic waveforms (e.g., Maguire et al., 2022) would provide a more real-

istic assessment but it is not considered feasible within the scope of this study. Insights from 3-D full wave synthetic tests conducted by Maguire et al. (2022) suggest that conventional surface wave travel time tomography is likely to underestimate the true magnitude of Vs reduction in crustal magma reservoirs, but the problem is more subdued for magma reservoirs that are large with respect to the inter-station spacing. In this study, the velocity anomaly of interest is ~6 km wide in the upper crust and the mean inter-station spacing is <1 km so we do not expect severe underestimation.

If the seismic properties are influenced by magmatic volatiles that could bias our interpretation of the melt-fraction toward over-estimation. Valles magmas may have several percent dissolved volatiles based on past eruptions (Boro et al., 2020; Waelkens et al., 2022). As magma cools in the upper crust buoyant volatiles may accumulate in a thin low-velocity layer atop the magma reservoir (e.g., Seccia et al., 2011). Such a scenario is plausible at Valles Caldera given that boreholes encountered high geothermal gradients up to 3.2 km deep (Figure 1) but did not reach magmatic fluids or recently cooled intrusions (Nielson and Hulen, 1984; Goff and Gardner, 1994), so some volatiles could be trapped beneath a low-permeability boundary. Resolution of a potential layer of magmatic volatiles atop a silicate melt reservoir may be possible with higher frequency Vp/Vs imaging, such as that conducted at Campi Flegrei, because lower Vp/Vs is expected for a trapped volume of exsolved volatiles compared to silicate melt (Calò and Tramelli, 2018; Chiarabba and Moretti, 2006). However, the paucity of seismicity beneath Valles caldera hinders the ability to conduct similar imaging. Comparison of teleseismic P-wave tomography and Rayleigh tomography is complicated by differing resolution, but the existing results do not suggest a low Vp/Vs anomaly since the Vs reduction (-32%) is greater than the Vp reduction (-23%) reported by Steck et al., (1998). A dominant role for exsolved volatiles in creating the low-velocity anomaly further seems unlikely because the high geothermal gradients in Valles Caldera are consistent with continued presence of melt (Nielsen and Hulen, 1984; Morgan et al., 1996).

Comparison of the Vs structure beneath Valles Caldera to that of other active silicic volcanic fields suggests an active magmatic system. The Laguna del Maule volcanic complex, which has hosted many Holocene rhyolite eruptions, exhibits similar Vs characteristics with a minimum Vs of ~2.0 km/s at ~4 km depth based on ambient noise Rayleigh wave tomography (Wespestad et al., 2019). Beneath Yellowstone Caldera the minimum Vs of ~2.8 km/s at ~5-10 km depth is faster than beneath Valles Caldera (Stachnik et al., 2008; Jiang et al., 2018), but the width of Yellowstone's upper crustal anomaly is up to ~60 km in comparison to the ~6 km width imaged here. Long Valley Caldera's seismically imaged reservoir appears deeper with a top at ~8 km and an underlying Vs anomaly extending to ~20 km depth with a minimum Vs of ~2.5 km/s (Nakata and Shelly, 2018; Flinders et al., 2018). Valles Caldera's Vs structure is more like the examples of Laguna del Maule and Yellowstone where the depth interval of the low-Vs anomaly largely overlaps typical pre-eruptive rhyolite storage depths of ~4-10 km (Bachmann and Bergantz, 2008). Given the 2D geometry of our

study we refrain from detailed estimates of the 3D volume of magma beneath Valles Caldera, but a simple approximation of a cylindrical volume with radius of 3 km and depth interval of 7 km would enclose most of the low-Vs anomaly. An ~20% melt fraction within the cylinder would correspond to ~40 km^3 of magma. Only a fraction of this volume would need to be mobilized to fuel eruptions analogous to those that produced the ~10 km^3 El Cajete pyroclastic deposits from ~74 ka or the ~4 km^3 Banco Bonito rhyolite flow from ~68 ka (Zimmerer et al., 2016; Wolff et al., 2011).

Evidence for upper crustal magma storage beneath Valles Caldera highlights challenges for hazard monitoring and research. Regional scale geophysical studies show that seismicity is locally absent beneath Valles Caldera (Nakai et al., 2017) and the adjacent Rio Grande Rift deforms slowly with an extension rate of ~0.1 mm/year (Berglund et al., 2012). Unlike similar settings in the United States such as Yellowstone Caldera or Long Valley Caldera, Valles Caldera does not have continuous open-access seismic or ground-based geodetic data. There is a local seismic network concentrated on the eastern flank of the caldera operated by Los Alamos National Laboratory (House and Roberts, 2020), but the data are not openly available and more spatially balanced coverage would be advantageous for detecting microseismicity beneath the caldera. Additionally, due to the lack of ground-based geodetic instruments, it is unclear whether the apparent lack of seismogenic deformation at Valles Caldera is accompanied by slower or ductile strain.

5 Conclusion

We have conducted the first local Vs tomography beneath Valles Caldera using ambient noise tomography with a dense linear array. A prominent low-Vs anomaly is focused within the 1.23 Ma caldera's ring fracture. It exhibits Vs reduction of ~32% and absolute Vs of ~2-2.1 km/s at depths of ~3-10 km coinciding with the depths of rhyolite storage for past eruptions. The upper crustal Vs reductions in the magma reservoir beneath Valles Caldera are similar or more severe than those at systems with more abundant evidence of seismicity or surface deformation. Our results indicate the potential importance of improved hazard monitoring capacity at Valles Caldera and, more generally, affirm that even seismically quiescent volcanic fields should be regarded as potential hosts of magma in the upper crust.

Acknowledgements

We acknowledge that the data for this research were collected on the unceded indigenous lands of the Pueblo and Ute peoples. We also acknowledge Santa Fe National Forest and Valles Caldera National Preserve, especially Research Coordinator Robert Parmenter, for facilitating land access for seismic data collection. Field workers are thanked for their efforts in collecting quality data. Fraser Goff, Peter Roberts, and Tobias Fischer engaged in helpful discussions throughout the study. This research was supported by NSF Grants EAR-2113315 (B. Schmandt) and EAR-2113367 (J. Chaput). Some of the seismic equipment used

in the study was provided by the IRIS PASSCAL Instrument Center and all the raw seismic data are archived at the IRIS Data Management Center; both facilities are supported through the Seismological Facilities for the Advancement of Geoscience (SAGE) Award of the NSF under Cooperative Support Agreement EAR-1851048.

Data Availability Statement

The ambient noise cross-correlation functions and inter-station phase velocities used for the tomography are openly archived (https://github.com/jwilgus/Valles_GRL). The raw seismic data for network 4E in 2019 are openly available from the IRIS Data Management Center (https://doi.org/10.7914/SN/4E_2019).

References

Ankeny, L. A., Braile, L. W., & Olsen, K. H. (1986). Upper crustal structure beneath the Jemez Mountains volcanic field, New Mexico, determined by three-dimensional simultaneous inversion of seismic refraction and earthquake data. Journal of Geophysical Research: Solid Earth, 91(B6), 6188-6198. https://doi.org/10.1029/JB091iB06p06188

Aprea, C. M., Hildebrand, S., Fehler, M., Steck, L., Baldridge, W. S., Roberts, P., ... & Lutter, W. J. (2002). Three-dimensional Kirchhoff migration: Imaging of the Jemez volcanic field using teleseismic data. Journal of Geophysical Research: Solid Earth, 107(B10), ESE-11.

Bachmann, O., & Bergantz, G. (2008). The magma reservoirs that feed supereruptions. *Elements*, *4*(1), 17-21.

Bensen, G. D., Ritzwoller, M. H., Barmin, M. P., Levshin, A. L., Lin, F., Moschetti, M. P., Shapiro, N.M., & Yang, Y. (2007). Processing seismic ambient noise data to obtain reliable broad-band surface wave dispersion measurements. Geophysical Journal International, 169(3), 1239-1260.

Berglund, H. T., Sheehan, A. F., Murray, M. H., Roy, M., Lowry, A. R., Nerem, R. S., & Blume, F. (2012). Distributed deformation across the Rio Grande rift, Great Plains, and Colorado plateau. Geology, 40(1), 23-26.

Berryman, J. G. (1980). Long-wavelength propagation in composite elastic media II. Ellipsoidal inclusions. *The Journal of the Acoustical Society of America*, *68*(6), 1820-1831.

Blomgren, V. J., Crossey, L. J., Karlstrom, K. E., Fischer, T. P., & Darrah, T. H. (2019). Hot spring hydrochemistry of the Rio Grande rift in northern New Mexico reveals a distal geochemical connection between Valles Caldera and Ojo Caliente. *Journal of Volcanology and Geothermal Research*, *387*, 106663.

Boro, J. R., Wolff, J. A., & Neill, O. K. (2020). Anatomy of a recharge magma: Hornblende dacite pumice from the rhyolitic Tshirege Member of the Bandelier Tuff, Valles Caldera, New Mexico, USA. *Contributions to Mineralogy and Petrology*, *175*(10), 1-26.

Brandon Schmandt. (2019). Valles 3C Node Transect [Data set]. International Federation of Digital Seismograph Networks. https://doi.org/10.7914/SN/4E_2019

Brocher, T. M. (2005). Empirical relations between elastic wavespeeds and density in the Earth's crust. Bulletin of the seismological Society of America, 95(6), 2081-2092.

Calò, M., & Tramelli, A. (2018). Anatomy of the Campi Flegrei caldera using enhanced seismic tomography models. *Scientific reports*, *8*(1), 1-12.

Cashman, K. V., & Giordano, G. (2014). Calderas and magma reservoirs. *Journal of Volcanology and Geothermal Research*, *288*, 28-45.

Chiarabba, C., & Moretti, M. (2006). An insight into the unrest phenomena at the Campi Flegrei caldera from Vp and Vp/Vs tomography. *Terra Nova*, *18*(6), 373-379.

Connolly, J. A. D. "The Geodynamic Equation of State: What and How." *Geochemistry, Geophysics, Geosystems* 10, no. 10 (2009). https://doi.org/10.1029/2009GC002540.

Cook, G. W., Wolff, J. A., & Self, S. (2016). Estimating the eruptive volume of a large pyroclastic body: the Otowi Member of the Bandelier Tuff, Valles caldera, New Mexico. *Bulletin of Volcanology*, *78*(2), 1-11.

Flinders, A.F., Shelly, D.R., Dawson, P.B., Hill, D.P., Tripoli, B., Shen, Y., 2018. Seismic evidence for significant melt beneath the Long Valley Caldera, California, USA. Geology 46 (9), 799–802.

Gardner, J. N., Goff, F., Garcia, S., & Hagan, R. C. (1986). Stratigraphic relations and lithologic variations in the Jemez volcanic field, New Mexico. Journal of Geophysical Research: Solid Earth, 91(B2), 1763-1778.

Goff, F., & Gardner, J. N. (1994). Evolution of a mineralized geothermal system, Valles Caldera, New Mexico. *Economic Geology*, *89*(8), 1803-1832.

Goff, F., Gardner, J. N., Reneau, S. L., Kelley, S. A., Kempter, K. A., & Lawrence, J. R. (2011). Geologic map of the Valles caldera, Jemez Mountains, New Mexico. New Mexico Bureau of Geology and Mineral Resources Geologic Map, 79(scale 1), 50.

Goff, F., & Janik, C. J. (2002). Gas geochemistry of the Valles caldera region, New Mexico and comparisons with gases at Yellowstone, Long Valley and other geothermal systems. *Journal of volcanology and geothermal research*, *116*(3-4), 299-323.

House, L., & Roberts, P. (2020). Seismicity Monitoring in North-Central New Mexico by the Los Alamos Seismic Network. Seismological Research Letters, 91(2A), 593-600. https://doi.org/10.1785/0220190208 https://doi.org/10.1785/0220190208

Huang, H. H., Lin, F. C., Schmandt, B., Farrell, J., Smith, R. B., & Tsai, V. C. (2015). The Yellowstone magmatic system from the mantle plume to the upper crust. Science, 348(6236), 773-776.

Jiang, C., Schmandt, B., Farrell, J., Lin, F. C., & Ward, K. M. (2018). Seismically anisotropic magma reservoirs underlying silicic calderas. *Geology*, *46*(8), 727-730.

Kennedy, B., Wilcock, J., & Stix, J. (2012). Caldera resurgence during magma replenishment and rejuvenation at Valles and Lake City calderas. *Bulletin of volcanology*, *74*(8), 1833-1847.

Kennett, B. L., Engdahl, E. R., & Buland, R. (1995). Constraints on seismic velocities in the Earth from traveltimes. *Geophysical Journal International*, *122*(1), 108-124.

Levshin, A.L., Yanovskaya, T.B., Lander, A.V., Bukchin B.G., Barmin, M.P., Ratnikova L.I., Its

E.N., 1989. Seismic Surface Waves in Laterally Inhomogeneous Earth. (Ed. V.I.Keilis-Borok), Kluwer Publ. House, Dordrecht/Boston/ London

Levshin, A. L., Pisarenko, V. F., & Pogrebinsky, G. A. (1972). On a frequency-time analysis of oscillations. In Annales de geophysique (Vol. 28, No. 2, pp. 211-218). Centre National de la Recherche Scientifique.

Maguire, R., Schmandt, B., Chen, M., Jiang, C., Li, J., & Wilgus, J. Resolving continental magma reservoirs with 3D surface wave tomography. Geochemistry, Geophysics, Geosystems, e2022GC010446.https://doi.org/10.1029/2022GC010446

Nakata, N., & Shelly, D. R. (2018). Imaging a crustal low-velocity layer using reflected seismic waves from the 2014 earthquake swarm at Long Valley Caldera, California: The magmatic system roof?. *Geophysical Research Letters*, *45*(8), 3481-3488.

Nasholds, M. W., & Zimmerer, M. J. (2022). High-precision 40Ar/39Ar geochronology and volumetric investigation of volcanism and resurgence following eruption of the Tshirege Member, Bandelier Tuff, at the Valles caldera. *Journal of Volcanology and Geothermal Research*, *431*, 107624.

Nielson, D. L., & Hulen, J. B. (1984). Internal geology and evolution of the Redondo dome, Valles caldera, New Mexico. Journal of Geophysical Research: Solid Earth, 89(B10), 8695-8711. https://doi.org/10.1029/JB089iB10p08695

Paulatto, M., Moorkamp, M., Hautmann, S., Hooft, E., Morgan, J. V., & Sparks, R. S. J. (2019). Vertically extensive magma reservoir revealed from joint inversion and quantitative interpretation of seismic and gravity data. *Journal of Geophysical Research: Solid Earth*, *124*(11), 11170-11191.

Phillips, E. H., Goff, F., Kyle, P. R., McIntosh, W. C., Dunbar, N. W., & Gardner, J. N. (2007). The 40Ar/39Ar age constraints on the duration of resurgence at the Valles caldera, New Mexico. *Journal of Geophysical Research: Solid Earth*, *112*(B8).

Roberts, P. M., Aki, K., & Fehler, M. C. (1991). A low-velocity zone in the basement beneath the Valles Caldera, New Mexico. Journal of Geophysical Research: Solid Earth, 96(B13), 21583-21596. https://doi.org/10.1029/91JB02048

Roberts, P. M., Aki, K., & Fehler, M. C. (1995). A shallow attenuating anomaly inside the ring fracture of the Valles Caldera, New Mexico. Journal of volcanology and geothermal research, 67(1-3), 79-99.https://doi.org/10.1016/0377-0273(94)00100-U

Sanford, A. R., Olsen, K. H., & Jaksha, L. H. (1979). Seismicity of the Rio Grande rift. Rio Grande Rift: Tectonics and Magmatism, 14, 145-168. https://doi.org/10.1029/SP014p0145

Schmandt, B., Jiang, C., & Farrell, J. (2019). Seismic perspectives from the western US on magma reservoirs underlying large silicic calderas. Journal of Volcanology and Geothermal Research, 384, 158-178.

Seats, K. J., Lawrence, J. F., & Prieto, G. A. (2012). Improved ambient noise correlation functions using Welch s method. *Geophysical Journal International*, *188*(2), 513-523.

Seccia, D., Chiarabba, C., De Gori, P., Bianchi, I., & Hill, D. P. (2011). Evidence for the contemporary magmatic system beneath Long Valley Caldera from local earthquake tomography and receiver function analysis. *Journal of Geophysical Research: Solid Earth*, *116*(B12).

Shen, W., Ritzwoller, M. H., Schulte-Pelkum, V., & Lin, F. C. (2013). Joint inversion of surface wave dispersion and receiver functions: a Bayesian Monte-Carlo approach. *Geophysical Journal International*, *192*(2), 807-836.

Spell, T. L., & Kyle, P. R. (1989). Petrogenesis of Valle Grande Member rhyolites, Valles Caldera, New Mexico: Implications for evolution of the Jemez Mountains Magmatic System. *Journal of Geophysical Research: Solid Earth*, *94*(B8), 10379-10396.

Stachnik, J. C., Dueker, K., Schutt, D. L., & Yuan, H. (2008). Imaging Yellowstone plume-lithosphere interactions from inversion of ballistic and diffusive Rayleigh wave dispersion and crustal thickness data. *Geochemistry, Geophysics, Geosystems*, *9*(6).

Steck, L. K., Thurber, C. H., Fehler, M. C., Lutter, W. J., Roberts, P. M., Baldridge, W. S., ... & Sessions, R. (1998). Crust and upper mantle P wave velocity structure beneath Valles caldera, New Mexico: results from the Jemez teleseismic tomography experiment. Journal of Geophysical Research: Solid Earth, 103(B10), 24301-24320. https://doi.org/10.1029/98JB00750

Szynkiewicz, A., Goff, F., Vaniman, D., & Pribil, M. J. (2019). Sulfur cycle in the Valles Caldera volcanic complex, New Mexico–Letter 1: Sulfate sources in aqueous system, and implications for S isotope record in Gale Crater on Mars. Earth and Planetary Science Letters, 506, 540-551.https://doi.org/10.1016/j.epsl.2018.10.036

Takei, Y. (2002). Effect of pore geometry on VP/VS: From equilibrium geometry to crack. *Journal of Geophysical Research: Solid Earth*, *107*(B2), ECV-6.

VanDecar, J. C., & Crosson, R. S. (1990). Determination of teleseismic relative phase arrival times using multi-channel cross-correlation and least squares. *Bulletin of the Seismological Society of America*, *80*(1), 150-169.

Waelkens, C. M., Stix, J., Eves, E., Gonzalez, C., & Martineau, D. (2022). H2O and CO2 evolution in the Bandelier Tuff sequence reveals multiple and discrete magma replenishments. *Contributions to Mineralogy and Petrology*, *177*(1), 1-23.

Wang, Y., Lin, F. C., Schmandt, B., & Farrell, J. (2017). Ambient noise tomography across Mount St. Helens using a dense seismic array. Journal of Geophysical Research: Solid Earth, 122(6), 4492-4508.

Wilcock, J., Goff, F., Minarik, W. G., & Stix, J. (2013). Magmatic recharge during the formation and resurgence of the Valles Caldera, New Mexico, USA: evidence from quartz compositional zoning and geothermometry. *Journal of Petrology*, *54*(4), 635-664.

Wilgus, J., Jiang, C., & Schmandt, B. (2020). A middle crustal channel of radial anisotropy beneath the northeastern Basin and range. *Tectonics*, *39*(7), e2020TC006140. https://doi.org/10.1029/2020TC006140

Wilson, C. J., Cooper, G. F., Chamberlain, K. J., Barker, S. J., Myers, M. L., Illsley-Kemp, F., & Farrell, J. (2021). No single model for supersized eruptions and their magma bodies. Nature Reviews Earth & Environment, 2(9), 610-627.

Wolff, J. A., Brunstad, K. A., & Gardner, J. N. (2011). Reconstruction of the most recent volcanic eruptions from the Valles caldera, New Mexico. *Journal of Volcanology and Geothermal Research*, *199*(1-2), 53-68.

Wolff, J. A., & Gardner, J. N. (1995). Is the Valles caldera entering a new cycle of activity? Geology, 23(5), 411-414. https://doi.org/10.1130/0091-7613(1995)023%3C0411:ITVCEA%3E2.3.CO;2

Wu, J., Cronin, S. J., Rowe, M. C., Wolff, J. A., Barker, S. J., Fu, B., & Boroughs, S. (2021). Crustal evolution leading to successive rhyolitic supereruptions in the Jemez Mountains volcanic field, New Mexico, USA. Lithos, 396, 106201. https://doi.org/10.1016/j.lithos.2021.106201

Zimmerer, M. J., Lafferty, J., & Coble, M. A. (2016). The eruptive and magmatic history of the youngest pulse of volcanism at the Valles caldera: Implications for successfully dating late Quaternary eruptions. Journal of Volcanology

and Geothermal Research, 310, 50-57.